# Energy & Environmental Science



## **PAPER**

View Article Online View Journal | View Issue

Cite this: Energy Environ. Sci., 2014, 7,

## The origin of high efficiency in low-temperature solution-processable bilayer organometal halide hybrid solar cells†

Shuangyong Sun,‡<sup>a</sup> Teddy Salim,‡<sup>a</sup> Nripan Mathews,<sup>abc</sup> Martial Duchamp,<sup>d</sup> Chris Boothroyd, Guichuan Xing, Tze Chien Sumbce and Yeng Ming Lam\*abf

This work reports a study into the origin of the high efficiency in solution-processable bilayer solar cells based on methylammonium lead iodide (CH3NH3PbI3) and [6,6]-phenyl-C61-butyric acid methyl ester (PC<sub>61</sub>BM). Our cell has a power conversion efficiency (PCE) of 5.2% under simulated AM 1.5G irradiation (100 mW cm<sup>-2</sup>) and an internal quantum efficiency of close to 100%, which means that nearly all the absorbed photons are converted to electrons and are efficiently collected at the electrodes. This implies that the exciton diffusion, charge transfer and charge collection are highly efficient. The high exciton diffusion efficiency is enabled by the long diffusion length of CH<sub>3</sub>NH<sub>3</sub>PbI<sub>3</sub> relative to its thickness. Furthermore, the low exciton binding energy of CH<sub>3</sub>NH<sub>3</sub>PbI<sub>3</sub> implies that exciton splitting at the CH<sub>3</sub>NH<sub>3</sub>Pbl<sub>3</sub>/PC<sub>61</sub>BM interface is very efficient. With further increase in CH<sub>3</sub>NH<sub>3</sub>Pbl<sub>3</sub> thickness, a higher PCE of 7.4% could be obtained. This is the highest efficiency attained for low temperature solutionprocessable bilayer solar cells to date.

Received 20th September 2013 Accepted 23rd October 2013

DOI: 10.1039/c3ee43161d

www.rsc.org/ees

#### **Broader context**

Low-temperature solution-processable bilayer solar cells with their simple architecture provide an inexpensive and straightforward platform for device fabrication without the necessity for extensive morphological optimization. For efficient solar cells, good light absorption accompanied by efficient conversion of photons to electrons is critical. This work shows that solar cells based on hybrid organic-inorganic lead halide as the donor and [6,6]-phenyl-C<sub>61</sub>-butyric acid methyl ester (PC<sub>61</sub>BM) as the acceptor are able to resolve the conflicting film thickness requirements of high absorption together with efficient exciton diffusion. As a result, practically all the photons absorbed by the active layer can be converted to electrons.

### Introduction

Low-temperature solution-processable solar cells are becoming more attractive as they offer a viable alternative to conventional solar cells fabricated via vacuum-based or high-temperature processes for large-scale, high-throughput and cost-effective

manufacturing on flexible plastic substrates. Despite the reported high performances, solar cells based on ternary or quaternary metal chalcogenides1,2 and dye-sensitized solar cells<sup>3</sup> generally require high-temperature processes (≥400 °C), restricting their compatibility with low heat-resistant polymer substrates. By contrast, organic/hybrid solar cells can be readily fabricated at low temperatures.4,5 Hybrid solar cells, which combine the advantages offered by both organic and inorganic materials, are also highly versatile in terms of the device structure they can adopt. Depending on how the photoactive layer is constructed, two basic solar cell device architectures can be obtained, i.e. bulk heterojunction (BHJ) and bilayer heterojunction. Bilayer solar cells have the merit of a more direct charge transport pathway at the expense of poorer exciton dissociation as compared to their BHJ counterpart. Furthermore, the bilayer solar cell with its simple architecture, essentially consisting of a stack of two photoactive layers, provides an inexpensive and straightforward platform for device fabrication without the necessity for extensive morphological optimization.

Very recently, semiconductors with the perovskite structure (ABX<sub>3</sub>) have become a popular class of materials for solar cells.

<sup>&</sup>lt;sup>a</sup>Nanyang Technological University, School of Materials Science and Engineering, 50 Nanyang Avenue, 639798, Singapore. E-mail: ymlam@ntu.edu.sg; Fax: +65 6790 9081 <sup>b</sup>Energy Research Institute @ NTU (ERI@N), 1 CleanTech Loop, #06-04 CleanTech One, Singapore 637141, Singapore

<sup>&#</sup>x27;Singapore-Berkeley Research Initiative for Sustainable Energy (SinBeRISE), 1 Create Way, Singapore 138602, Singapore

<sup>&</sup>lt;sup>d</sup>Ernst Ruska-Centrum und Peter Grünberg Institut, Forschungszentrum Jülich, D-52425 Jülich, Germany

<sup>&</sup>lt;sup>e</sup>Division of Physics and Applied Physics, School of Physical and Mathematical Sciences, Nanyang Technological University, 21 Nanyang Link, Singapore 637371, Singapore

<sup>&</sup>lt;sup>f</sup>Institute of Materials for Electronic Engineering II, RWTH-Aachen, Sommerfeldstr. 24, D-52074 Aachen, Germany

<sup>†</sup> Electronic supplementary information (ESI) available. See DOI: 10.1039/c3ee43161d

<sup>‡</sup> The authors contributed equally.

Hybrid organic-inorganic lead halide (e.g. CH<sub>3</sub>NH<sub>3</sub>PbX<sub>3</sub>, X = halogen) perovskites with good intrinsic optoelectronic properties have been synthesized and used for photovoltaic cell applications. 6-11 These hybrid perovskites are also commonly, perhaps inappropriately, referred to as organometal halide/ trihalide. The highest efficiency of perovskite solar cells to date was 15.4% reported by Liu et al. which has a planar heterojunction architecture with vapour-deposited perovskite sandwiched between TiO2 and spiro-OMeTAD.12 In another study, Lee et al. demonstrated that CH<sub>3</sub>NH<sub>3</sub>PbI<sub>2</sub>Cl in conjunction with spiro-OMeTAD could work as both a light absorber and an electron conductor.8 On the other hand, Etgar et al. demonstrated that CH3NH3PbI3 can act simultaneously as an efficient light harvester and transport holes in CH3NH3PbI3/ TiO<sub>2</sub> hybrid heterojunction solar cells. It is also possible to finetune the bandgap of CH3NH3PbX3 by varying the chemical composition of the material, resulting in a range of device performance and stability.10 Despite the great excitement in the solar cell field, the application of CH3NH3PbX3 for lowtemperature-processable solar cells is very limited at present. The previous reported works mostly employ mesoporous oxide layers and hole blocking layers that require high-temperature processing. Hence, an avenue towards the utilization of these materials for low-temperature processable solar cells has to be identified. The pairing of CH<sub>3</sub>NH<sub>3</sub>PbX<sub>3</sub> with the other electron acceptors other than inorganic metal oxides also has not been much explored and hence, investigation of alternative materials may open up new possibilities in this area. Bilayer devices provide a straightforward platform to assess the compatibility between CH3NH3PbX3 and novel acceptor materials. Furthermore, due to the versatility of organometal halides in transporting both holes and electrons, it is possible that with the right combination of materials, bilayer devices based on organometal halides will perform efficiently. Very recently, Eperson et al. demonstrated that a CH<sub>3</sub>NH<sub>3</sub>PbI<sub>3-r</sub>Cl<sub>r</sub> based solar cell containing no mesoporous layer with well controlled morphology can achieve a PCE above 10%, which shows planar heterojunction perovskite solar cells have the advantage of simple architecture hence ease of fabrication.14

In this contribution, we demonstrate the outstanding planar device performance and investigate the origin of the high efficiency in these solution-processable solar cells based on methylammonium lead iodide (CH3NH3PbI3) and [6,6]-phenyl-C<sub>61</sub>-butyric acid methyl ester (PC<sub>61</sub>BM) in a bilayer configuration: ITO/PEDOT:PSS/CH<sub>3</sub>NH<sub>3</sub>PbI<sub>3</sub>/PC<sub>61</sub>BM/Al. CH<sub>3</sub>NH<sub>3</sub>PbI<sub>3</sub> and PC<sub>61</sub>BM behave as the electron donor (D) and acceptor (A), respectively. This simple planar heterojunction solar cell exhibits a remarkable performance, giving a PCE of 5.23% with a short-circuit current ( $I_{SC}$ ) of 8.201 mA cm<sup>-2</sup>, an open-circuit voltage  $(V_{\rm OC})$  of 0.824 V and a fill factor (FF) of 0.774 under simulated AM 1.5G irradiation (100 mW cm<sup>-2</sup>). By employing a thicker CH<sub>3</sub>NH<sub>3</sub>PbI<sub>3</sub> layer, a much higher PCE of 7.41% with J<sub>SC</sub> of 10.829 mA cm $^{-2}$ ,  $V_{\rm OC}$  of 0.905 V and FF of 0.756 can be obtained. To date, this is the most efficient low-temperature solution-processable bilayer solar cell. The high performance of our device is found to be the result of the high internal quantum efficiency (IQE) of close to 100%, indicating that almost every absorbed photon can be successfully converted to free charge carriers that can be efficiently collected at the electrodes. Besides the appealing facile all-solution-processability, we note that our bilayer device is also ultrathin and can be processed at low temperatures (<150 °C) rendering it compatible with flexible substrates and lightweight applications.

#### Results and discussion

Methylammonium lead iodide (CH3NH3PbI3) film was formed via spincoating of an equimolar mixture of CH3NH3I and PbI2 precursor solutions. The film was heat-treated at 100 °C and was further characterized by X-ray diffraction (XRD). The appearance of strong peaks at  $2\theta = 13.95^{\circ}$ ,  $28.35^{\circ}$  and  $31.70^{\circ}$  (ESI, Fig. S1†), corresponding to the (110), (220) and (310) planes, indicates the formation of the tetragonal perovskite structure. 15,16 After verifying that CH<sub>3</sub>NH<sub>3</sub>PbI<sub>3</sub> was successfully synthesized, we coupled it with the n-type organic semiconductor PC<sub>61</sub>BM to make the bilayer solar cells. Fig. 1 shows the device structure of the hybrid CH<sub>3</sub>NH<sub>3</sub>PbI<sub>3</sub>/PC<sub>61</sub>BM solar cell and the energy level diagram of the respective device components. As seen from the energy level diagram, the combination of these two active materials yields a type-II heterojunction. The CH<sub>3</sub>NH<sub>3</sub>PbI<sub>3</sub> film was first deposited on poly(3,4-ethylenedioxythiophene):poly(styrenesulfonate) (PEDOT:PSS)-coated indium tin oxide (ITO) substrates and was subsequently heated at 100 °C for 30 s. It is imperative to note that heat treatment is essential for a complete conversion from precursor to final organolead halide. It was found that

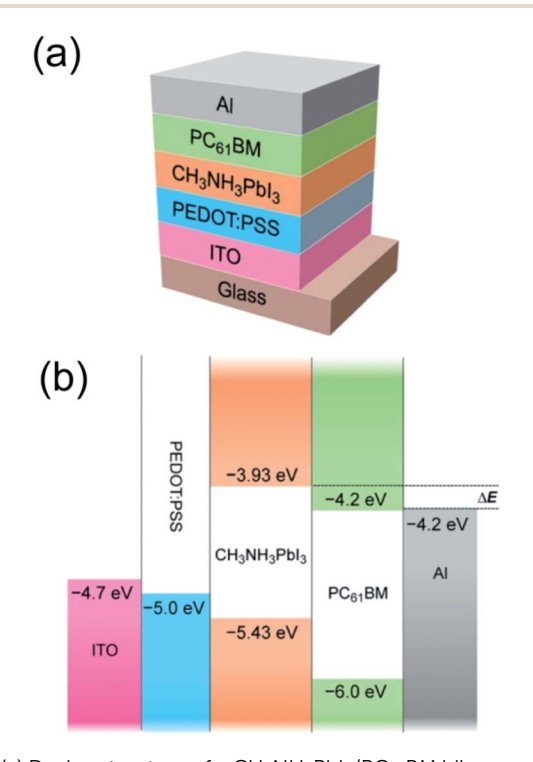
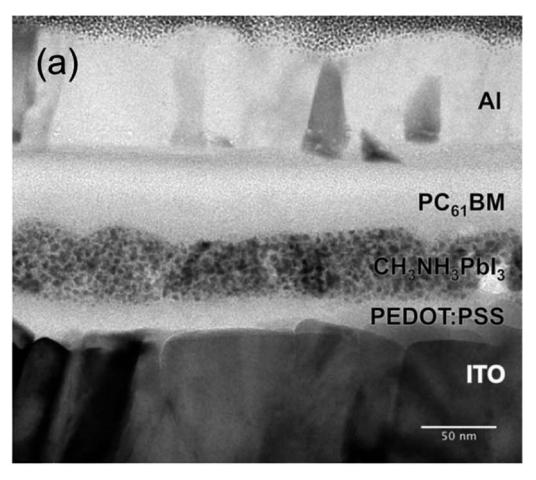


Fig. 1 (a) Device structure of a CH<sub>3</sub>NH<sub>3</sub>PbI<sub>3</sub>/PC<sub>61</sub>BM bilayer solar cell. (b) Schematic energy level diagram of ITO, PEDOT:PSS, CH<sub>3</sub>NH<sub>3</sub>Pbl<sub>3</sub>, PC<sub>61</sub>BM and Al. The energy levels are taken from Kim et al.<sup>6</sup> and Thompson & Fréchet. 13 The energy offset is noted at  $\Delta E$ .

heating the film at 100 °C for as short as 30 s was sufficient to achieve this purpose. The heat-treated CH<sub>3</sub>NH<sub>3</sub>PbI<sub>3</sub> film exhibits better optical absorption, higher crystallinity and an increase in interfacial area for exciton dissociation, all of which lead to an enhancement of device performance. The effect of heat treatment is discussed in detail in the ESI.† Next, the PC<sub>61</sub>BM layer was spincoated onto the heat-treated CH<sub>3</sub>NH<sub>3</sub>PbI<sub>3</sub> layer. The CH<sub>3</sub>NH<sub>3</sub>PbI<sub>3</sub> and PC<sub>61</sub>BM are soluble in polar and non-polar solvents, respectively. Solvent orthogonality ensures that the CH3NH3PbI3 film remains intact after PC61BM deposition. No heat treatment was applied after coating with the PC61BM film to prevent interdiffusion between the two materials at the heterojunctions. Eventually, an aluminum cathode was deposited on the active layer through a shadow mask. Our device fabrication methodology is highly compatible with lowtemperature processes, emphasizing its potential for costeffective, flexible solar cells.

Fig. 2 shows a bright field cross-sectional transmission electron microscope (TEM) image of our device and a high resolution TEM (HRTEM) image of the crystalline CH<sub>3</sub>NH<sub>3</sub>PbI<sub>3</sub> layer. The ultrathin cross-sectional sample was prepared using a



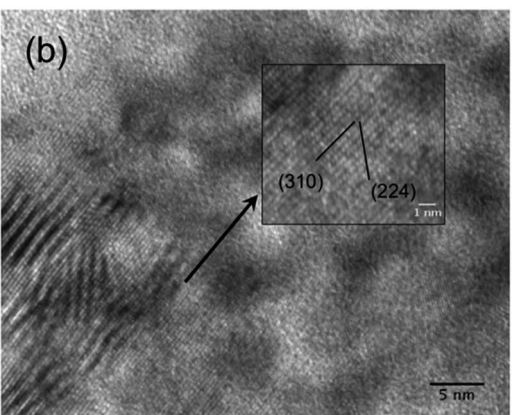


Fig. 2 (a) Bright-field TEM cross-sectional image of the ITO/ PEDOT:PSS/CH<sub>3</sub>NH<sub>3</sub>PbI<sub>3</sub>/PC<sub>61</sub>BM/Al bilayer solar cell. (b) HRTEM image of the CH<sub>3</sub>NH<sub>3</sub>Pbl<sub>3</sub> layer. The (310) and (224) lattice planes are identified in the inset. The cross-section sample was prepared using

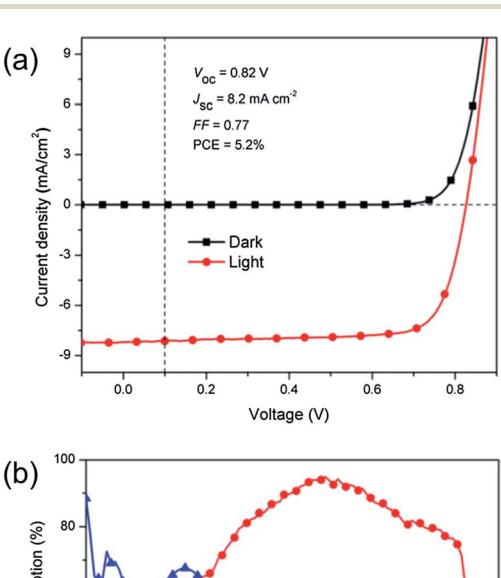
focused ion beam (FIB). In the TEM image (Fig. 2a), distinct layers with different features and contrast can be observed, confirming that our fabricated devices indeed have a planar junction architecture with a small donor-acceptor interface area. While previous work on organolead halide only employs this material deposited on inorganic meso-superstructures, 6-8,10,11 we note that a standalone compact CH<sub>3</sub>NH<sub>3</sub>PbI<sub>3</sub> film can also be implemented for solar cells. Essentially, our CH<sub>3</sub>NH<sub>3</sub>PbI<sub>3</sub> layer has great similarity to the solid organolead halide "capping layer" observed by Ball et al. 17 The thin layer of CH<sub>3</sub>NH<sub>3</sub>PbI<sub>3</sub> contains many dark spots corresponding to high atomic number crystalline material. The adjacent bright layers, below and above the CH3NH3PbI3 layer, are PEDOT:PSS and PC<sub>61</sub>BM. As observed, PC<sub>61</sub>BM forms a continuous layer on CH<sub>3</sub>NH<sub>3</sub>PbI<sub>3</sub> and the interface between them is not diffuse. Similar features with reversed contrast can be seen in the annular dark-field scanning transmission electron microscopy (ADF-STEM) image (ESI, Fig. S2†). The HRTEM image of the CH<sub>3</sub>NH<sub>3</sub>PbI<sub>3</sub> layer (Fig. 2b) reveals lattice fringes, which correspond to the planes from the intercalating PbI<sub>2</sub> and CH<sub>3</sub>NH<sub>2</sub>I, surrounded by some amorphous regions. The lattice planes correspond to those observed by XRD (ESI, Fig. S1†). The darker contrast observed could indicate either a few overlapping crystallite planes or the existence of planes with different orientations. Unlike crystalline CH<sub>3</sub>NH<sub>3</sub>PbI<sub>3</sub> quantum dots previously reported to form on TiO2 surfaces, 16,18 we note that our deposition yields polycrystalline regions throughout the CH<sub>3</sub>NH<sub>3</sub>PbI<sub>3</sub> film. From Fig. 2a, it can be seen that both the  $CH_3NH_3PbI_3$  and the  $PC_{61}BM$  layers have a thickness of 50  $\pm$ 5 nm, which agrees well with the thickness measured using a surface profilometer. It is also noticeable that our CH<sub>3</sub>NH<sub>3</sub>PbI<sub>3</sub>/ PC<sub>61</sub>BM bilayer is significantly thinner than the previously reported systems on organolead halide perovskite (>300 nm). To further confirm the material in each distinct layer and to verify that no interdiffusion occurs in the bilayer device, EDS spectra were collected from all the layers as shown in ESI Fig. S3.†

We note that the interface between PEDOT:PSS and CH<sub>3</sub>NH<sub>3</sub>PbI<sub>3</sub>, which is analogous to the other hybrid Schottky diodes, 19-21 could potentially act as heterojunction for exciton dissociation due to the existence of an internal electric field at the interface. In that case, the holes are transferred to the Fermi level  $(E_{\rm F})$  of PEDOT:PSS, while the electrons are transferred to the conduction-band minimum  $(E_C)$  of  $CH_3NH_3PbI_3$ . In order to investigate these possibilities, we performed steady state photoluminescence (PL) measurements on CH3NH3PbI3 only, CH<sub>3</sub>NH<sub>3</sub>PbI<sub>3</sub>/PEDOT:PSS and CH<sub>3</sub>NH<sub>3</sub>PbI<sub>3</sub>/PC<sub>61</sub>BM bilayers. As indicated in ESI Fig. S4,† the PL intensity is quenched by a factor of 4 when coupled with the PEDOT:PSS layer and is further quenched by an additional factor of 3 in the CH<sub>3</sub>NH<sub>3</sub>PbI<sub>3</sub>/PC<sub>61</sub>BM heterojunction. This evidently indicates the efficacy of both junctions in splitting the excitons generated in CH<sub>3</sub>NH<sub>3</sub>PbI<sub>3</sub> with PC<sub>61</sub>BM being a superior electron acceptor, which agrees with the recent finding by Abrusci et al.<sup>22</sup>

To determine the feasibility of PC<sub>61</sub>BM as electron acceptor in our planar heterojunction configuration, we compared CH3NH3PbI3 perovskite devices with and without a PC61BM layer. The devices were not based on our optimized fabrication

conditions. The current density-voltage (J-V) characteristics of their respective devices are provided in ESI Fig. S5.† In the absence of PC<sub>61</sub>BM, the ITO/PEDOT:PSS/CH<sub>3</sub>NH<sub>3</sub>PbI<sub>3</sub>/Al device does not exhibit any meaningful power that could be extracted from the fourth quadrant of the light *J-V* characteristic graph. The fact that there is no significant photovoltaic characteristic observable in the ITO/PEDOT:PSS/CH<sub>3</sub>NH<sub>3</sub>PbI<sub>3</sub>/Al device, despite the reported ambipolar characteristics of organolead halide and its use as an n-type transporter, 8,17,23 suggests that either the PEDOT:PSS/CH3NH3PbI3 interface is less efficacious in promoting exciton dissociation and charge transfer, which correlates with the PL data, or the positioning of the electronic levels of the device components is unfavorable for both charge transport and collection. On the other hand, the device with the PC<sub>61</sub>BM layer demonstrates typical photovoltaic behavior with a short-circuit current ( $J_{SC}$ ) of 5.961 mA cm<sup>-2</sup>, open-circuit voltage  $(V_{\rm OC})$  of 0.832 V, fill factor (FF) of 0.671 and power conversion efficiency (PCE) of 3.33%. The lack of efficient exciton dissociating interfaces in the absence of n-type PC<sub>61</sub>BM in one of the devices compared to the other is responsible for the remarkable difference in device performance of the two types of devices.24

The thickness of CH<sub>3</sub>NH<sub>3</sub>PbI<sub>3</sub> layers can be controlled by varying the concentration of the organolead halide solution and the deposition parameters. The best performing device was obtained using a 9 wt% precursor solution and no interlayer



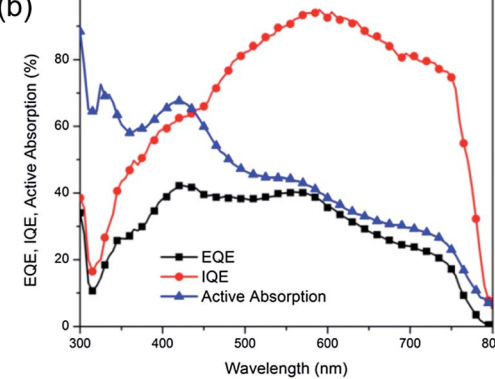


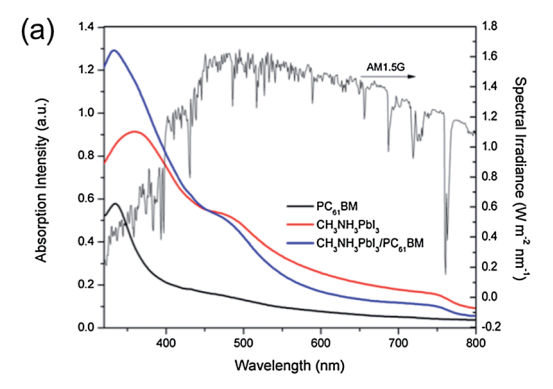
Fig. 3 (a) Current density–voltage (J-V) characteristics of ITO/PEDOT:PSS/CH<sub>3</sub>NH<sub>3</sub>Pbl<sub>3</sub>/PC<sub>61</sub>BM/Al bilayer solar cell in dark and under AM 1.5G illumination. (b) EQE, IQE and active absorption spectra of the ITO/PEDOT:PSS/CH<sub>3</sub>NH<sub>3</sub>Pbl<sub>3</sub>/PC<sub>61</sub>BM/Al bilayer solar cell.

was applied between the  $PC_{61}BM$  and the Al. Fig. 3a demonstrates the J-V characteristics of our best  $CH_3NH_3PbI_3/PC_{61}BM$  bilayer solar cell device in dark and under AM 1.5G illumination (100 mW cm<sup>-2</sup>). The optimum device exhibits outstanding performance with a  $J_{SC}$  of 8.201 mA cm<sup>-2</sup>,  $V_{OC}$  of 0.824 V, FF of 0.774 and PCE of 5.23%. To the best of our knowledge, this is one of the highest reported efficiencies for a low-temperature solution-processable solar cell with a genuine bilayer architecture. During the course of our manuscript preparation, Jeng et al. reported a similar system with an efficiency of 3.9% and with a lower FF and  $V_{OC}$ , <sup>25</sup> attributable to the roughness of the  $CH_3NH_3PbI_3$  films. The planarity of their interface was also not verified.

The high J<sub>SC</sub> measured in CH<sub>3</sub>NH<sub>3</sub>PbI<sub>3</sub>/PC<sub>61</sub>BM, which is atypical of organic/hybrid bilayer devices, could be an amalgam of a few factors: (1) a large optical absorption coefficient, (2) a wide absorption window, (3) a moderate exciton diffusion length and (4) excellent charge-carrier mobility. We calculated the absorption coefficient (α) of a CH<sub>3</sub>NH<sub>3</sub>PbI<sub>3</sub> film on a quartz substrate based on the methodology developed by Cesaria et al.,26 which realistically accounts for the non-measurable contribution of the film-substrate interface. The calculated  $\alpha$ for the  $CH_3NH_3PbI_3$  perovskite film is  $4.3 \times 10^5$  cm<sup>-1</sup> at 360 nm (ESI, Fig. S6†), which is approximately an order of magnitude higher than the previously reported value by Im et al.16 They estimated the  $\alpha$  of CH<sub>3</sub>NH<sub>3</sub>PbI<sub>3</sub> to be 1.5  $\times$  10<sup>4</sup> cm<sup>-1</sup> at 550 nm, while our calculation yields  $\alpha$  to be 1.3  $\times$  10<sup>5</sup> cm<sup>-1</sup> in the same wavelength range. The inconsistency in the  $\alpha$  values could be ascribed to the fact that Im et al. performed their measurement on CH<sub>3</sub>NH<sub>3</sub>PbI<sub>3</sub>-coated TiO<sub>2</sub> samples and in that case, the measurement included the contribution of  $TiO_2$ . The  $\alpha$  of CH3NH3PbI3 is comparable to or even higher than many conjugated molecules commonly used in highly efficient organic solar cell devices.27-29 As compared to inorganic semiconductors, e.g.  $\text{Cu}_2\text{ZnSnS}_4$  ( $\alpha \approx 6.1 \times 10^4 \text{ cm}^{-1}$  at 650 nm)<sup>30</sup> or CuInSe<sub>2</sub> ( $\alpha = 6 \times 10^5 \text{ cm}^{-1} \text{ at 690 nm}$ ), CH<sub>3</sub>NH<sub>3</sub>PbI<sub>3</sub> has a very similar range of absorption coefficient. Due to the reasonably high  $\alpha$  of CH<sub>3</sub>NH<sub>3</sub>PbI<sub>3</sub> in the visible region, it is possible to form a sufficiently thin yet strongly absorbing film, which is crucial to a bilayer device.

Furthermore, the optical bandgap of  ${\rm CH_3NH_3PbI_3}$  ( $E_{\rm g}\approx 1.5~{\rm eV}$ ) corresponds well to the bandgap requirement of an ideal single p–n junction solar cell.<sup>32</sup> The absorption of the organolead halide perovskite extends throughout the UV-visible region with an absorption onset at ca. 790 nm (Fig. 4a). The  ${\rm CH_3NH_3PbI_3}$  film exhibits an absorption peak at ca. 360 nm and a "shoulder" band at ca. 480 nm. On the other hand, the  ${\rm CH_3NH_3PbI_3/PC_{61}BM}$  bilayer, in which both layers have a similar range of thickness, exhibits superposed absorption characteristics of its constituents. The broad absorption window overlapping with the maximum irradiance of the solar spectrum ensures efficient photon harvesting, which may eventually lead to a high photocurrent.

Fig. 3b shows the active absorption, external quantum efficiency (EQE) and internal quantum efficiency (IQE) curves from our best CH<sub>3</sub>NH<sub>3</sub>PbI<sub>3</sub>/PC<sub>61</sub>BM device. The absorption was measured directly on an ITO/PEDOT:PSS/CH<sub>3</sub>NH<sub>3</sub>PbI<sub>3</sub>/PC<sub>61</sub>BM/



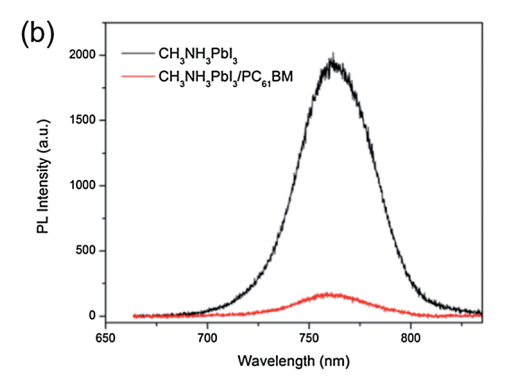


Fig. 4 (a) UV-vis absorption spectra from the CH<sub>3</sub>NH<sub>3</sub>Pbl<sub>3</sub>/PC<sub>61</sub>BM bilayer and its constituents. The AM 1.5G spectral irradiance is also included for comparison. (b) Steady-state PL spectra for CH<sub>3</sub>NH<sub>3</sub>Pbl<sub>3</sub> and  $CH_3NH_3PbI_3/PC_{61}BM$  ( $\lambda_{ex}=600$  nm).

Al bilayer device based on the technique proposed by Burkhard et al.,33 as detailed in the ESI.† The parasitic absorption spectra and the derivation of the active layer absorption are shown in ESI Fig. S7.† The CH<sub>3</sub>NH<sub>3</sub>PbI<sub>3</sub>/PC<sub>61</sub>BM absorption characteristics obtained from the device via the semi-empirical approach slightly differ from those acquired from the bilayer film alone (Fig. 4a). It is plausible that optical interference effects induce the wavelength-dependent exciton generation profiles to have maxima at different spots in the device (ESI, Fig. S8†). Consequently, the fraction of photoabsorption in each layer is different, attributed to the alteration of the "effective" absorption of the bilayer. As shown in Fig. 3b, the CH<sub>3</sub>NH<sub>3</sub>PbI<sub>3</sub>/PC<sub>61</sub>BM device exhibits an EQE (charge extracted per incident photon), as high as 41% at ca. 570 nm. The integration of EQE spectra yields  $J_{
m SC}$  of 8.04 mA cm $^{-2}$ , approximately <2% different from the value measured under AM 1.5G illumination. The measurement of IQE, i.e. charge extracted per photon absorbed, provides some insight into the possible operating mechanism of our CH<sub>3</sub>NH<sub>3</sub>PbI<sub>3</sub>/PC<sub>61</sub>BM bilayer device and the origin of the high PCE thereof. It decouples the contribution of photon absorption and is a practical gauge in assessing the effectiveness of bilayer architecture to generate photocurrent. The IQE can be written as

$$\eta_{\rm IQE} = \eta_{\rm ED} \times \eta_{\rm CT} \times \eta_{\rm CC} \tag{1}$$

where  $\eta_{\rm ED}$  is exciton diffusion efficiency,  $\eta_{\rm CT}$  is charge transfer efficiency and  $\eta_{CC}$  is charge collection efficiency. The IQE is

conventionally larger than the EQE, which is also observed in our bilayer device (Fig. 3b) and was calculated by considering both the EQE and the active absorption. The IQE of the CH3NH3PbI3/ PC<sub>61</sub>BM bilayer device is above 90% throughout the wavelength range of 550-650 nm with an IQE<sub>max</sub> of 95% at ca. 580 nm. Interestingly, this wavelength range corresponds to the local maxima of the electric fields in the CH<sub>3</sub>NH<sub>3</sub>PbI<sub>3</sub> layer, as shown in our simulation results (ESI, Fig. S9†). In general, a high IQE > 80% is observable in nearly the entire visible spectrum (490-750 nm). Such a remarkable IQE (approaching unity) indicates that almost every absorbed photon is converted into a pair of charge-carriers and that almost all charge-carriers generated are efficiently collected at both electrodes. Ball et al. have also demonstrated an IQE close to 100% for their Cl-doped CH<sub>3</sub>NH<sub>3</sub>PbI<sub>3</sub> solar cells, although their IOE was not derived directly from the EOE and was instead estimated from the device photocurrent  $(I_{SC})^{17}$ 

The surprisingly high IQE in our bilayer device can be explained by evaluating the three factors that IQE is dependent on. Firstly, the exciton diffusion length  $(L_D)$  is comparable to the thickness of the perovskite layer (≥50 nm). In comparison, the  $L_{\rm D}$  in conjugated polymers is reported to be in the range of 2-10 nm.<sup>34-36</sup> Besides, the exciton lifetime (τ) in pure CH<sub>3</sub>NH<sub>3</sub>PbI<sub>3</sub> powder is exceptionally high, up to 78 ns; while  $\tau$  for singlet excitons in organic semiconductors is much shorter (<5 ns).37 The combination of these two effects means that the excitons in the CH<sub>3</sub>NH<sub>3</sub>PbI<sub>3</sub> film can travel a longer distance before decay, increasing their likelihood of reaching the heterojunction to dissociate into free electron-hole pairs.

Secondly, there is an efficient charge transfer from the CH<sub>3</sub>NH<sub>3</sub>PbI<sub>3</sub> to the PC<sub>61</sub>BM at the interface. This is evident from the efficient photoluminescence (PL) quenching of CH<sub>3</sub>NH<sub>3</sub>PbI<sub>3</sub> (>90%) in the presence of PC<sub>61</sub>BM (Fig. 4b). The efficient PL quenching at the CH<sub>3</sub>NH<sub>3</sub>PbI<sub>3</sub>/PC<sub>61</sub>BM interface, which is comparable to that observed in nanoscale phase-separated polymer-fullerene BHJs,38,39 is indicative of an efficient exciton diffusion in CH3NH3PbI3 to the dissociating interface, followed by an efficient electron transfer to the fullerene phase. The exciton binding energy  $(E_b)$ , which greatly impacts the efficiency of exciton dissociation and charge transfer, was elucidated temperature-dependent photoluminescence

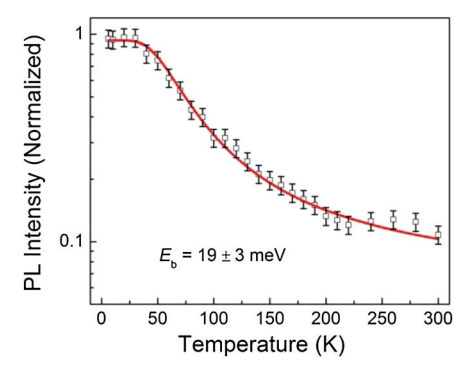


Fig. 5 Temperature-dependent integrated PL intensity of the CH<sub>3</sub>NH<sub>3</sub>PbI<sub>3</sub> film under excitation of a 532 nm continuous-wave laser beam. The solid line is the best fit based on the Arrhenius equation.

measurements. From the plot of the integrated PL intensity as a function of temperature (Fig. 5), a least square fit of the data with the Arrhenius equation  $(I(T) = I_0/(1 + Ae^{(-E_b/k_BT)}))$  yields an exciton binding energy of 19  $\pm$  3 meV. This indicates that an electric field is still required to dissociate all the excitons generated but as this value is much lower than that of typical organic semiconductors (>100 meV),40 the electric field required to split the excitons is much lower. The overall driving force to promote exciton dissociation and electron transfer from the CH3NH3PbI3 donor to the PC<sub>61</sub>BM acceptor is provided by the energy offset between the conduction-band minimum (E<sub>C</sub>) of CH<sub>3</sub>NH<sub>3</sub>PbI<sub>3</sub> and the lowestunoccupied molecular orbital (LUMO) of PC61BM. From the energy level diagram (Fig. 1b), it can be seen that the energy offset ( $\Delta E = 0.27$  eV) is more than 10-fold higher than the  $E_b$  of CH<sub>3</sub>NH<sub>3</sub>PbI<sub>3</sub>, suggesting that the internal field at the heterointerface is indisputably sufficient for exciton dissociation. This results in a nearly instantaneous exciton splitting at the interface preceding the electron transfer to the fullerene phase. Furthermore, the deep LUMO level of C60 derivatives tends to induce high electron affinity towards electron donating materials, promoting a favorable charge transfer.41 The holes in CH3NH3PbI3 and the electrons in PC61BM eventually drift towards the anode (ITO) and cathode (Al), respectively.

Thirdly, it is important to consider the long-range charge transport and efficient charge collection. The subsequent charge transport is also not an issue as the pathways of holes to the anode and electrons to the cathode are well defined and continuous. On top of that, the high hole mobility ( $\mu_h \approx 0.6~{\rm cm}^2~{\rm V}^{-1}~{\rm s}^{-1}$ )<sup>42</sup> of metal halide perovskite and the high electron mobility ( $\mu_e \approx 1~{\rm cm}^2~{\rm V}^{-1}~{\rm s}^{-1}$ )<sup>43</sup> of PC<sub>61</sub>BM have been reported based on field-effect transistor measurements. Ball *et al.* have also observed effective charge transport and collection in their CH<sub>3</sub>NH<sub>3</sub>PbX<sub>3</sub> devices, in which the thick organolead halide layer did not adversely affect the device performance. Therefore, the charge recombination in our CH<sub>3</sub>NH<sub>3</sub>PbI<sub>3</sub>/PC<sub>61</sub>BM bilayer device is expected to be low.

Besides a high  $J_{SC}$ , the other two factors responsible for the highly efficient CH<sub>3</sub>NH<sub>3</sub>PbI<sub>3</sub>/PC<sub>61</sub>BM bilayer device are its impressive  $V_{\rm OC}$  and FF. The high  $V_{\rm OC}$  of 0.824 V is comparable to those reported for "champion" organic solar cells based on low bandgap materials, e.g. PTB7:PCBM ( $V_{OC} = 0.74 \text{ V}$ ), 44 PBDTTT-CF:PCBM  $(V_{OC} = 0.76 \text{ V})^{45}$  and PCDTBT:PCBM  $(V_{OC} = 0.88 \text{ CF})^{45}$ V). In comparison, wide bandgap P3HT only gives a  $V_{\rm OC}$  of  $\sim$ 0.6 V when coupled with PCBM. 46 Coincidentally, the  $V_{\rm OC}$  of CH<sub>3</sub>NH<sub>3</sub>PbI<sub>3</sub>/PC<sub>61</sub>BM lines up agreeably in comparison with the abovementioned devices, following the monotonic trend of highest-occupied molecular orbital (HOMO) or valence-band maximum  $(E_{\rm V})$  levels of the donor materials (i.e. -5 eV, -5.15 eV, -5.22 eV, -5.43 eV and -5.5 eV for P3HT, PTB7, PBDTTT-CF, CH<sub>3</sub>NH<sub>3</sub>PbI<sub>3</sub> and PCDTBT, respectively). It has been reported that the  $V_{\rm OC}$  of blend organic solar cells is empirically governed by the following relationship

$$V_{\rm OC} \approx (1/e)(|E_{\rm HOMO}^{\rm donor}| - |E_{\rm LUMO}^{\rm acceptor}|)$$
 (2)

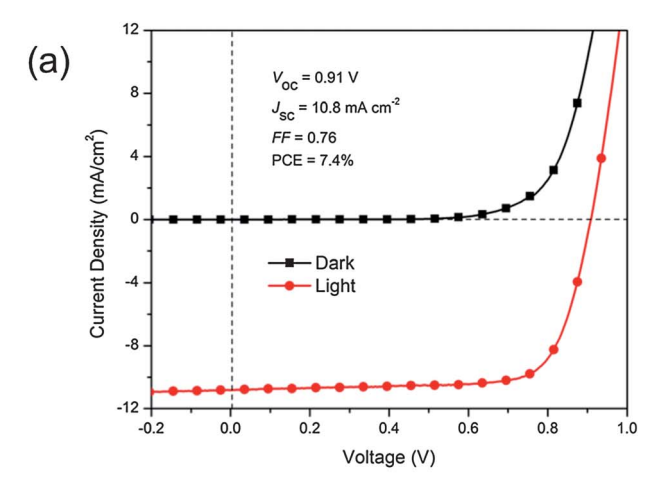
where  $E_{\text{HOMO}}^{\text{donor}}$  is the HOMO level of the donor and  $E_{\text{LUMO}}^{\text{acceptor}}$  is the LUMO level of the acceptor.<sup>47</sup> Since CH<sub>3</sub>NH<sub>3</sub>PbI<sub>3</sub> has a

deep-lying  $E_{\rm V}$  (or HOMO-equivalent) level, the device is expected to yield a high photovoltage. Our result also emphasizes the feasibility of estimating the  $V_{\rm OC}$  of both metal halide perovskite/fullerene bilayers and blend devices.

Our CH<sub>3</sub>NH<sub>3</sub>PbI<sub>3</sub>/PC<sub>61</sub>BM bilayer solar cell has a magnificent FF of up to 0.774 and is among the highest reported for solution-deposited solar cells. This value is remarkable as highly efficient solution-processable solar cells with wellengineered electrode interfaces so far have only shown FF values of 0.60-0.72.4,45,48 By contrast, we did not apply any electron-transport layer (ETL) to assist charge collection. The high FF indicates that the charge transport and collection of the bilayer solar cells are very efficient, corresponding well with the high IQE. It also implies that the charge recombination in this bilayer system is not an efficiency-limiting issue. It is well known that the FF parameter is closely related to both the series resistance  $(R_s)$  and the shunt resistance  $(R_{sh})$  of solar cells. From the slope of the J-V curve around the open-circuit and shortcircuit regions,  $R_s$  and  $R_{sh}$  are calculated to be 6.4  $\Omega$  cm<sup>2</sup> and 1.6 k $\Omega$  cm<sup>2</sup>, respectively. The low  $R_s$  is usually associated with efficient charge transport with negligible charge accumulation and recombination.

Throughout this contribution, we have shown that in our bilayer solar cell device based on an ITO/PEDOT:PSS/ CH<sub>3</sub>NH<sub>3</sub>PbI<sub>3</sub>/PC<sub>61</sub>BM/Al configuration, CH<sub>3</sub>NH<sub>3</sub>PbI<sub>3</sub> works as the main light absorber, electron donor (D) and p-type (hole) conductor, while PC61BM acts as the electron acceptor (A) and n-type (electron) conductor. The photogenerated excitons in the CH<sub>3</sub>NH<sub>3</sub>PbI<sub>3</sub> layer get dissociated at the D/A interfaces. The holes in the CH<sub>3</sub>NH<sub>3</sub>PbI<sub>3</sub> and electrons in the PC<sub>61</sub>BM eventually drift towards and are collected at the anode (ITO) and cathode (Al), respectively. The PC61BM also helps in preventing a direct contact between the highly conductive CH3NH3PbI3  $(\sim 10^{-3} \text{ S cm}^{-3})^9$  and the top electrode. The PEDOT:PSS layer essentially smoothens the ITO surface and assists the hole transport from CH<sub>3</sub>NH<sub>3</sub>PbI<sub>3</sub> to ITO. It is also demonstrated that a PCE in excess of 5% could be obtained from the bilayer CH<sub>3</sub>NH<sub>3</sub>PbI<sub>3</sub>/PC<sub>61</sub>BM device. In comparison, solutiondeposited organic solar cells with discernible planar interfaces usually suffer from poor PCEs (<2%) attributed to the short exciton diffusion length. 49,50 It is necessary to differentiate between pure bilayer and "pseudo" bilayer; the latter manifests from either a thermally driven interdiffusion between both layers51-53 or a simple sandwiching of a heterogeneous layer between two homogeneous layers.54,55 Due to the difference in device geometry, i.e. a lack of well-defined planar heterointerfaces, "pseudo" bilayer devices are not comparable with these CH<sub>3</sub>NH<sub>3</sub>PbI<sub>3</sub>/PC<sub>61</sub>BM bilayer devices.

Despite the remarkable performance, it is imperative to point out that the  $CH_3NH_3PbI_3$  absorption in our bilayer system is yet to be optimized. As seen earlier, the EQE obtained from our  $CH_3NH_3PbI_3/PC_{61}BM$  bilayer device is noticeably lower than the reported values for the other organolead halide perovskite devices (EQE > 60%),<sup>7,8,10</sup> and this likely due to our poorer perovskite absorption. We surmise that the enhancement in optical absorption should lead to higher EQE and hence  $J_{SC}$ . To attest this hypothesis, similar devices were prepared with



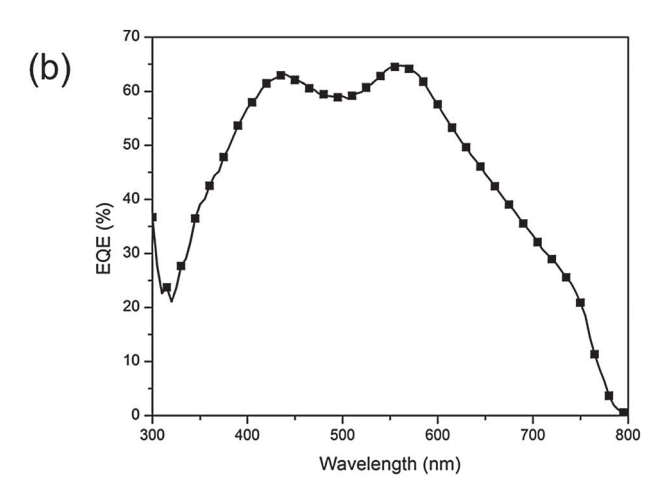


Fig. 6 (a) Current density-voltage (J-V) characteristics of ITO/ PEDOT:PSS/CH<sub>3</sub>NH<sub>3</sub>PbI<sub>3</sub>/PC<sub>61</sub>BM/Al bilayer solar cell with thicker CH<sub>3</sub>NH<sub>3</sub>PbI<sub>3</sub> in dark and under AM 1.5G illumination. (b) EQE spectra of the corresponding ITO/PEDOT:PSS/CH3NH3Pbl3/PC61BM/Al bilayer solar cell.

thicker CH<sub>3</sub>NH<sub>3</sub>PbI<sub>3</sub> films (110 ± 5 nm) on PEDOT:PSS following the procedures reported by Burschka et al.11 This approach involves two-step deposition of each organolead halide precursor, as opposed to the one-step deposition of the mixture of precursors previously employed. A significant improvement in photocurrent was observed as shown in Fig. 6a. The device showed a  $J_{SC}$  of 10.829 mA cm<sup>-2</sup>,  $V_{OC}$  of 0.905 V, FF of 0.756 and PCE of 7.41%. This is nearly twice as high as the results obtained by Jeng et al. with a comparable device structure.  $^{25}$  The higher  $J_{\rm SC}$  is also confirmed by a much higher EQE of 65% at ca. 550 nm (Fig. 6b). Liu et al. reported  $J_{SC}$  in excess of 20 mA cm<sup>-2</sup> with an organolead halide layer of more than 300 nm. <sup>12</sup> Therefore, further enhancement in  $J_{\rm SC}$ , which is the pivotal parameter in our PCE improvement, can be expected for our bilayer system if the main absorber layer, i.e. CH<sub>3</sub>NH<sub>3</sub>PbI<sub>3</sub>, is made even thicker. Besides absorption optimization, it will also be interesting to couple organolead halide perovskite with the other types of fullerene derivatives, with either better absorption characteristics to induce higher photocurrent or better energetics to improve photovoltage. Lastly, for long-term

practical use of bilayer devices, they should be subjected to stability tests to validate their reliability.

#### Conclusions

In summary, we have demonstrated a pure bilayer CH<sub>3</sub>NH<sub>3</sub>PbI<sub>3</sub>/ PC<sub>61</sub>BM solar cell which has excellent performance with a PCE of 7.4%, the best reported to date for an all-solution-processable planar heterojunction device. The active layer is sufficiently thin (<100 nm) and the device can be fabricated with lowtemperature processes (<150 °C). Furthermore, a bilayer system is also desirable due to its simplicity in processing. The high performance of the bilayer device can be attributed to the high IQE of close to unity (100%), suggesting that the exciton diffusion, charge transfer and charge collection are highly efficient. The high fill factor of 77% is also one of the best reported for organic and hybrid solar cells. Through further optimization of photon harvesting, an improvement in PCE to beyond 10% is within reach.

## Experimental section

#### Materials

Methylammonium iodide (CH3NH3I) was synthesized according to reported procedures.16 To prepare the organolead halide perovskite precursor solution, as-synthesized CH<sub>3</sub>NH<sub>3</sub>I powder and lead(II) iodide powder (PbI2, Aldrich) were mixed in anhydrous dimethylformamide (DMF, Aldrich) with a weight ratio of 1:3. The suspension (9 wt%) was stirred overnight at 60 °C. Prior to device fabrication, the precursor solution was filtered with a 0.45 μm PVDF filter. [6,6]-Phenyl-C<sub>61</sub>-butyric acid methyl ester (PC<sub>61</sub>BM) was purchased from Nano-C®. PC<sub>61</sub>BM (10 mg mL<sup>-1</sup>) was dissolved in a solvent mixture of anhydrous chlorobenzene (CB, Aldrich) and anhydrous chloroform (CF, Aldrich) (CB : CF = 1 : 1 v/v). All materials were used directly without purification.

#### Device fabrication and characterization

Solar cells were fabricated on indium tin oxide (ITO)-coated glass substrates (Xinyan Technology Ltd., 7  $\Omega$  sq<sup>-1</sup>) with the following device configuration: ITO/PEDOT:PSS/CH3NH3PbI3/ PC<sub>61</sub>BM/Al. The ITO-coated glass substrates were successively cleaned in detergent, deionized water, acetone and isopropanol in an ultrasonic bath for 15 min each. Subsequently, the substrates were plasma-cleaned for 2 min before being coated with a 30 nm-thick PEDOT:PSS (CleviosTM Al 4083) layer. Afterwards the substrates were baked at 140 °C for 10 min in a N<sub>2</sub> filled glove box. Perovskite precursor solution was spincoated on the PEDOT:PSS layer at 3000 rpm for 40 s. The films were subsequently heated at 100 °C for 30 s. The CH<sub>3</sub>NH<sub>3</sub>PbI<sub>3</sub> samples were always subjected to thermal treatment by default, unless other processing conditions are specified. The PC61BM layer was then spin-coated onto the CH<sub>3</sub>NH<sub>3</sub>PbI<sub>3</sub> layer at 1200 rpm for 60 s to generate the bilayer. No heat treatment was done on the PC61BM layer. Finally an aluminum cathode (100 nm) was deposited on the active layer

through a shadow mask to give a device area of  $0.07~{\rm cm}^2$  under a vacuum level of  $10^{-6}$  torr. Approximately 20 devices were fabricated for each experimental variable.

The current density-voltage (J-V) characteristics of the devices were measured in darkness and under Air Mass 1.5 Global (AM 1.5G) illumination (SAN-EI Electric) using a Keithley SMU 2400 source meter. The light intensity was first calibrated to 100 mW cm<sup>-2</sup> with a digital Solar Meter (Daystar, DS-05A). External quantum efficiency (EQE) measurement was done with a Merlin radiometer (Newport) with a monochromator-calibrated wavelength control. The light was coupled into an optical cable (Ocean Optics). A calibrated silicon photodiode (Hamamatsu) was used as a reference device in counting incident photons. All device measurements were performed in an inert  $N_2$  environment.

#### **Materials characterization**

Optical absorbance spectra of perovskite films on quartz and total reflectance of the device were measured using a UV-vis-NIR spectrophotometer (Shimadzu UV-3600) with an integrating sphere (ISR-3100). The internal quantum efficiency (IQE) of the device was calculated according to the reported literature. The total absorption of the device was calculated from the measured reflectance spectrum of the device. Parasitic absorption was calculated using a transfer matrix formalism to evaluate the absorptions not in the active layer. For the modeling, the refractive indices (n, k) of the materials were either obtained from the literature or measured with an ellipsometer. The active absorption from the active layer was obtained by subtracting the modeled parasitic absorption from the total absorption. Afterwards, the IQE was calculated based on the measured EQE and the active absorption.

The crystal structure of the CH<sub>3</sub>NH<sub>3</sub>PbI<sub>3</sub> perovskite film was investigated with an X-ray diffractometer (XRD, Bruker D8 Advance) equipped with a  $Cu-K_{\alpha}$  X-ray tube. The acquisition was carried out in the range  $10\text{--}60^{\circ}$  in  $\theta\text{--}2\theta$  mode with a scan angle of 1° using a step size of 0.04° and a time step of 3 s. The surface morphology of the perovskite was imaged with tapping-mode atomic force microscopy (AFM, Asylum MFP-3D-BIO). An Al reflex coated AFM probe (Olympus AC240TS) with a spring constant of 2 N m<sup>-1</sup> and tip radius of 9 nm was used. TEM cross-section samples were prepared using a standard lift-out procedure in a dual-beam FEI Helios focused ion beam (FIB) workstation. Two consecutive protective layers of ~100 nm of electron-beam-deposited Pt and  $\sim$ 1  $\mu m$  of ion-beam-deposited Pt were used to avoid degradation of the samples due to Ga<sup>2+</sup> implantation during milling. Coarse FIB milling was carried out using a 30 kV ion beam, while final milling was performed at 5 kV ion energy. The angular dark-field scanning transmission electron microscope (ADF-STEM) imaging was performed in a FEI Helios electron microscope (15 kV FEG) and high-resolution transmission electron microscope (HR-TEM) images were obtained using a Philips CM20 TEM (200 kV, FEG) and a FEI Titan (300 kV, FEG). The EDX characterization was performed using a Philips CM20 TEM and an EDAX detector. The thickness of the CH<sub>3</sub>NH<sub>3</sub>PbI<sub>3</sub> film was measured with both an Alpha-Step profiler (KLA-Tencor) and an AFM.

For time-integrated photoluminescence (PL) measurements, the light source was a Coherent Legend<sup>TM</sup> regenerative amplifier (150 fs, 1 kHz, 800 nm) that was seeded by a Coherent Vitesse™ oscillator (100 fs, 80 MHz). 600 nm, 150 fs laser pulses were generated from a Coherent TOPAS-C optical parametric amplifier. The laser pulses were directed to the films which were put in vacuum. The fluence was kept to a minimum of  $\sim$ 1.3  $\mu$ J cm<sup>-2</sup> per pulse to avoid any second order effects in the dynamics. The emission from the samples was collected at a backscattering angle of 150° by a pair of lenses and into an optical fiber that was coupled to a spectrometer (Acton, Spectra Pro 2500i) to be detected by a charge-coupled device (Princeton Instruments, Pixis 400B). To determine the exciton binding energy, the temperature dependent PL was conducted with the same experimental geometry but with a continuous excitation light source (532 nm,  $\sim$ 1 mJ cm<sup>-2</sup>).

## Acknowledgements

The authors also would like to especially thank Dr Eric T. Hoke for discussion on the transfer matrix calculation, Drs Chuan Seng Tan and Kwang Hong Lee for the ellipsometry measurement and Ms Jeannette M. Kadro for her help in the synthesis of CH<sub>3</sub>NH<sub>3</sub>I. The authors acknowledge the Energy Research Institute (a) NTU (ERI(a)N) for the use of the facilities. M.D. acknowledges financial support from the European Union under the Seventh Framework Programme under a contract for an Integrated Infrastructure Initiative (reference 312483 – ESTEEM2). T.C.S. acknowledges the support from the following research grants: NTU start-up grant (M58110068); a Competitive Research Programme grant (NRF-CRP5-2009-04) and the Singapore-Berkeley Research Initiative for Sustainable Energy (SinBeRISE) CREATE Programme. Y.M.L. acknowledges the support from The Danish Council for Strategic Research.

#### References

- 1 Q. Guo, G. M. Ford, R. Agrawal and H. W. Hillhouse, *Progress in Photovoltaics: Research and Applications*, 2013, **21**, 64–71.
- 2 T. K. Todorov, J. Tang, S. Bag, O. Gunawan, T. Gokmen, Y. Zhu and D. B. Mitzi, *Adv. Energy Mater.*, 2013, 3, 34–38.
- 3 A. Yella, H.-W. Lee, H. N. Tsao, C. Yi, A. K. Chandiran, M. K. Nazeeruddin, E. W.-G. Diau, C.-Y. Yeh, S. M. Zakeeruddin and M. Grätzel, *Science*, 2011, 334, 629–634.
- 4 Z. He, C. Zhong, S. Su, M. Xu, H. Wu and Y. Cao, *Nat. Photonics*, 2012, **6**, 591–595.
- 5 J. You, L. Dou, K. Yoshimura, T. Kato, K. Ohya, T. Moriarty, K. Emery, C.-C. Chen, J. Gao, G. Li and Y. Yang, *Nat. Commun.*, 2013, 4, 1446.
- 6 H.-S. Kim, C.-R. Lee, J.-H. Im, K.-B. Lee, T. Moehl, A. Marchioro, S.-J. Moon, R. Humphry-Baker, J.-H. Yum, J. E. Moser, M. Gratzel and N.-G. Park, *Sci. Rep.*, 2012, 2, 1–7.
- 7 J. H. Heo, S. H. Im, J. H. Noh, T. N. Mandal, C.-S. Lim, J. A. Chang, Y. H. Lee, H.-j. Kim, A. Sarkar, K. NazeeruddinMd, M. Gratzel and S. I. Seok, *Nat. Photonics*, 2013, 7, 486–491.

- 8 M. M. Lee, J. Teuscher, T. Miyasaka, T. N. Murakami and H. J. Snaith, Science, 2012, 338, 643-647.
- 9 L. Etgar, P. Gao, Z. Xue, Q. Peng, A. K. Chandiran, B. Liu, M. K. Nazeeruddin and M. Grätzel, J. Am. Chem. Soc., 2012, 134, 17396-17399.
- 10 J. H. Noh, S. H. Im, J. H. Heo, T. N. Mandal and S. I. Seok, Nano Lett., 2013, 13, 1764-1769.
- 11 J. Burschka, N. Pellet, S.-J. Moon, R. Humphry-Baker, P. Gao, M. K. Nazeeruddin and M. Gratzel, Nature, 2013, 499, 316-
- 12 M. Liu, M. B. Johnston and H. J. Snaith, Nature, 2013, 501, 395-398.
- 13 B. C. Thompson and J. M. J. Fréchet, Angew. Chem., Int. Ed., 2008, 47, 58-77.
- 14 G. E. Eperon, V. M. Burlakov, P. Docampo, A. Goriely and H. J. Snaith, Adv. Funct. Mater., 2013, DOI: 10.1002/ adfm.201302090.
- 15 A. Kojima, K. Teshima, Y. Shirai and T. Miyasaka, J. Am. Chem. Soc., 2009, 131, 6050-6051.
- 16 J.-H. Im, C.-R. Lee, J.-W. Lee, S.-W. Park and N.-G. Park, Nanoscale, 2011, 3, 4088-4093.
- 17 J. M. Ball, M. M. Lee, A. Hey and H. J. Snaith, Energy Environ. Sci., 2013, 6, 1739-1743.
- 18 J.-H. Im, J. Chung, S.-J. Kim and N.-G. Park, Nanoscale Res. Lett., 2012, 7, 353.
- 19 S.-C. Shiu, J.-J. Chao, S.-C. Hung, C.-L. Yeh and C.-F. Lin, Chem. Mater., 2010, 22, 3108-3113.
- 20 F. Zhang, T. Song and B. Sun, Nanotechnology, 2012, 23, 194006.
- 21 J.-J. Chao, S.-C. Shiu, S.-C. Hung and C.-F. Lin, Nanotechnology, 2010, 21, 285203.
- 22 A. Abrusci, S. D. Stranks, P. Docampo, H.-L. Yip, A. K. Y. Jen and H. J. Snaith, Nano Lett., 2013, 13, 3124-3128.
- 23 E. Edri, S. Kirmayer, D. Cahen and G. Hodes, J. Phys. Chem. Lett., 2013, 4, 897-902.
- 24 C. W. Tang, Appl. Phys. Lett., 1986, 48, 183-185.
- 25 J.-Y. Jeng, Y.-F. Chiang, M.-H. Lee, S.-R. Peng, T.-F. Guo, P. Chen and T.-C. Wen, Adv. Mater., 2013, 25, 3727-3732.
- 26 M. Cesaria, A. P. Caricato and M. Martino, J. Opt., 2012, 14, 105701.
- 27 B. Walker, C. Kim and T.-Q. Nguyen, Chem. Mater., 2010, 23, 470-482.
- 28 S. H. Park, A. Roy, S. Beaupre, S. Cho, N. Coates, J. S. Moon, D. Moses, M. Leclerc, K. Lee and A. J. Heeger, Nat. Photonics, 2009, 3, 297–302.
- 29 Y. Kim, S. Cook, S. M. Tuladhar, S. A. Choulis, J. Nelson, J. R. Durrant, D. D. C. Bradley, M. Giles, I. McCulloch, C.-S. Ha and M. Ree, *Nat. Mater.*, 2006, 5, 197–203.
- 30 K. Ito and T. Nakazawa, Jpn. J. Appl. Phys., 1988, 27, 2094-2097.
- 31 L. L. Kazmerski, M. Hallerdt, P. J. Ireland, R. A. Mickelsen and W. S. Chen, J. Vac. Sci. Technol., A, 1983, 1, 395-398.
- 32 W. Shockley and H. J. Queisser, J. Appl. Phys., 1961, 32, 510-519.

- 33 G. F. Burkhard, E. T. Hoke and M. D. McGehee, Adv. Mater., 2010, 22, 3293-3297.
- 34 D. E. Markov, C. Tanase, P. W. M. Blom and J. Wildeman, Phys. Rev. B: Condens. Matter Mater. Phys., 2005, 72, 045217.
- 35 J. E. Kroeze, T. J. Savenije, M. J. W. Vermeulen and J. M. Warman, J. Phys. Chem. B, 2003, 107, 7696-7705.
- 36 P. E. Shaw, A. Ruseckas and I. D. W. Samuel, Adv. Mater., 2008, 20, 3516-3520.
- 37 M. R. Narayan and J. Singh, Phys. Status Solidi C, 2012, 9, 2386-2389.
- 38 M. Hallermann, I. Kriegel, E. Da Como, J. M. Berger, E. von Hauff and J. Feldmann, Adv. Funct. Mater., 2009, 19, 3662-3668.
- 39 H. Wang, H.-Y. Wang, B.-R. Gao, L. Wang, Z.-Y. Yang, X.-B. Du, O.-D. Chen, J.-F. Song and H.-B. Sun, Nanoscale, 2011, 3, 2280-2285.
- 40 V. I. Arkhipov and H. Bässler, Phys. Status Solidi A, 2004, 201, 1152-1187.
- 41 P. M. Allemand, A. Koch, F. Wudl, Y. Rubin, F. Diederich, M. M. Alvarez, S. J. Anz and R. L. Whetten, J. Am. Chem. Soc., 1991, 113, 1050-1051.
- 42 C. R. Kagan, D. B. Mitzi and C. D. Dimitrakopoulos, Science, 1999, 286, 945-947.
- 43 T. B. Singh, N. Marjanović, G. J. Matt, S. Günes, N. S. Sariciftci, A. Montaigne Ramil, A. Andreev, H. Sitter, R. Schwödiauer and S. Bauer, Org. Electron., 2005, 6, 105-110.
- 44 Y. Liang, Z. Xu, J. Xia, S.-T. Tsai, Y. Wu, G. Li, C. Ray and L. Yu, Adv. Mater., 2010, 22, E135-E138.
- 45 H.-Y. Chen, J. Hou, S. Zhang, Y. Liang, G. Yang, Y. Yang, L. Yu, Y. Wu and G. Li, Nat. Photonics, 2009, 3, 649-653.
- 46 G. Li, V. Shrotriya, J. Huang, Y. Yao, T. Moriarty, K. Emery and Y. Yang, Nat. Mater., 2005, 4, 864-868.
- 47 M. C. Scharber, D. Mühlbacher, M. Koppe, P. Denk, C. Waldauf, A. J. Heeger and C. J. Brabec, Adv. Mater., 2006, 18, 789-794.
- 48 C. E. Small, S. Chen, J. Subbiah, C. M. Amb, S.-W. Tsang, T.-H. Lai, J. R. Reynolds and F. So, Nat. Photonics, 2012, 6, 115-120.
- 49 A. L. Ayzner, C. J. Tassone, S. H. Tolbert and B. J. Schwartz, J. Phys. Chem. C, 2009, 113, 20050-20060.
- 50 K. H. Lee, P. E. Schwenn, A. R. G. Smith, H. Cavaye, P. E. Shaw, M. James, K. B. Krueger, I. R. Gentle, P. Meredith and P. L. Burn, Adv. Mater., 2011, 23, 766-770.
- 51 V. S. Gevaerts, L. J. A. Koster, M. M. Wienk and R. A. J. Janssen, ACS Appl. Mater. Interfaces, 2011, 3, 3252-3255.
- 52 A. Loiudice, A. Rizzo, M. Biasiucci and G. Gigli, J. Phys. Chem. Lett., 2012, 3, 1908-1915.
- 53 D. Chen, F. Liu, C. Wang, A. Nakahara and T. P. Russell, Nano Lett., 2011, 11, 2071-2078.
- 54 J. Xue, B. P. Rand, S. Uchida and S. R. Forrest, Adv. Mater., 2005, 17, 66-71.
- 55 X. Xiao, J. D. Zimmerman, B. E. Lassiter, K. J. Bergemann and S. R. Forrest, Appl. Phys. Lett., 2013, 102, 073302.